Theoretical Study of the Reaction $CH(X^2\Pi) + NO(X^2\Pi)$. I. Determination of Some Reaction Paths in the Lowest Triplet Potential Energy Surface

N. Marchand, P. Jimeno, J. C. Rayez,* and D. Liotard

Laboratoire de Physicochimie Théorique, URA 503/CNRS, Université Bordeaux I, Domaine Universitaire, 33405 Talence Cedex, France

Received: January 13, 1997; In Final Form: May 29, 1997[⊗]

In this paper, which is the first of a series devoted to some aspects of the title reaction, we present the theoretical results concerning the topology of the lowest potential energy surface of triplet multiplicity. Results at the ab initio CASPT2 level with a complete active space self-consistent field (CASSCF) reference wave function built on a D95 Dunning basis set and involving 10 electrons in 10 orbitals are reported. This triplet surface is expected to play an important role in this reaction since experimental results show $HCN(X^1\Sigma^+)$ as the main product, and this product can only be obtained via an $HCNO(^3A)$ hypersurface. We find that the channel leading to the formation of $HCN(X^1\Sigma^+) + O(^3P)$ is the most likely product channel, in agreement with available experimental findings. To a lesser extent, we can also observe the formation of the product channels $HCO(X^2A') + N(^4S)$, $NCO(X^2\Pi) + H(^2S)$, and $CO(X^1\Sigma^+) + NH(X^3\Sigma^-)$. Conversely, the formation of $CN(X^2\Sigma^+) + OH(X^2\Pi)$ is highly unlikely because of the existence of high potential energy barriers along this reaction path.

I. Introduction

Nitrogen oxides are among the major atmospheric pollutants released by combustion processes. One way to minimize their harmful effects is to chemically reduce them before their release in the atmosphere by the reburning of combustion products in an excess of hydrocarbon. Lanier et al.[1] as well as Chen et al.[2] have reported significant reductions in NO_x emission in a pilot scale power plant through this method of reburning with hydrocarbons. However, optimization of such processes demands a better understanding of the nitrogen chemistry in the reburning zones. The initial steps of the NO reburning processes are not well established. Miller and Bowman[3] have investigated the mechanism of the NO → HCN → N_2 conversion during combustion with different hydrocarbons, identifying the initiation reactions of the reburning processes to be C + NO → CN + O and CH + NO → HCN + O. In a general way, the reactions of CH_x + NO are believed to play a crucial role in the overall reburning mechanism. Among such reactions, CH + NO has a special interest from a theoretical point of view since it is the simplest system involving four different atoms. Several experimental determinations of the overall rate constant of this reaction have been reported in the literature.[4−10] All agree in their estimates of the rate of disappearance of CH and NO at 300 K, yielding $k(300\ \text{K}) \approx 2.0 \times 10^{-10}$ cm^3 molecule^{-1} s^{-1} as an average. However, very little is known about the rate constants of formation of the possible product channels at this temperature. This reaction is also likely to occur in interstellar chemistry, since it has a rate constant approaching the gas kinetic limit, and the molecule HNCO has recently been detected in the galactic center.[11,12]

Six chemical rearrangement channels are thermodynamically open at 300 K, being presented in Table 1. Each channel, leading to the formation of diatomic and triatomic fragments in different electronic states, is expected to play a role in the kinetics and in the dynamics of the reaction CH + NO. The exoergicities $\Delta\epsilon_0$ (difference between the zero-point energy level of the products and the zero-point energy level of the reactants) correspond to the formation of the ground electronic state products when several electronic states are present. The determination of the relevant branching ratio is required to broaden the understanding of the NO reburning processes. Dean et al.[8] and Miller and Bowman[3] have both observed HCN + O as the most likely product channel in shock tube studies performed over the temperature range 2600−3800 K. In more recent work, Lambrecht et al.,[13] using time-resolved infrared diode laser absorption spectroscopy to measure the branching ratio of the CD + NO reaction, found a 47.5% yield for the DCN + O channel, a smaller yield for the three channels NCO + D, CO + ND, and DCO + N, and almost no CN + OD products. Bozzelli et al.,[14] using a quantum version of the RRK method,[15] predicted HCN + O as the most probable products followed by HCO + N and NCO + H. In agreement with all the previous experimental results, Takezaki and co-workers[16] proposed the formation of HCN and/or OH as main products by a spectroscopic analysis. Although some divergences occur among the results concerning the branching ratios of the available products, all agree in claiming that the formation of HCN is the most likely product channel.

TABLE 1: Exothermic Channels Associated with the $CH(X^2\Pi) + NO(X^2\Pi)$ Reaction[a]

products	$-\Delta\epsilon_0$ (eV)	$-\Delta\epsilon_0$ (kcal mol^{-1})
$H(^2S) + CNO(X^2\Pi)$	0.60	13.84
$N(^4S) + HCO(X^2A', A^2A'')$	1.75	40.36
$OH(X^2\Pi) + CN(X^2\Sigma^+, A^2\Pi_i)$	2.18	50.27
$O(^3P) + HCN(X^1\Sigma^+)$	3.11	71.72
$H(^2S) + NCO(X^2\Pi, A^2\Sigma^+)$	3.18	73.33
$CO(X^1\Sigma^+) + NH(X^3\Sigma^-, a^1\Delta, b^1\Sigma^+, A^3\Pi)$	4.86	112.08

[a] Experimental exoergicities $\Delta\epsilon_0$ concern the most exothermic channel when several electronic states of the products are specified. These values are obtained from Takezaki et al.[16]

Several ab initio calculations were carried out 20 years ago on the singlet potential energy surface (PES) of the isomers of isocyanic acid (HNCO) by Poppinger et al.,[17] and, more recently, some specific stable CHNO structures have been studied by Yokoyama et al.,[18] East et al.,[19] and Pinnavaia and co-workers.[20] While this article was in preparation, Mebel et al.[21] published

[⊗] Abstract published in *Advance ACS Abstracts,* July 15, 1997.

S1089-5639(97)00203-X CCC: $14.00

a paper on a theoretical density functional theory (DFT) study of the potential energy surfaces in singlet and triplet multiplicities of CHNO, using the hybrid density functional B3LYP method to investigate the PES.

This paper is the first of a series concerning the theoretical study of the reaction between CH and NO.[22] The ultimate goal is 2-fold: (i) the determination of the kinetic parameters (preexponential factor, activation energy, and rate constant) of all the possible channels involved in this reaction at 300 K and (ii) the study of the dynamics of these processes. Comparisons with experimental results will be possible since the kinetic and dynamic aspects of this reaction are also being studied experimentally here in Bordeaux.[23a]

To obtain information on the kinetics, the first step is the theoretical determination of the different reaction paths which connect the reagents to the products. This is the subject of this paper, which deals mainly with a search for the minima and saddle points in the lowest triplet energy surface. As further study of the dynamics will require an analytical description[24] of the different PES involved in this reaction, we decided to use a reliable ab initio approach of moderate computing cost, since we will have to calculate a large number of points. In order to avoid a blind research of the topology of the surfaces, we used, as a guide, a semiempirical approach of the lowest potential energy surfaces involved in the reaction $CH(X^2\Pi) + NO(X^2\Pi)$. Obviously, it is well known that semiempirical approaches cannot give reliable quantitative results about energies, but it is clear that the topological features of the PES such as the existence of minima or saddle points are, most of the time, well reproduced by a "good" semiempirical approach like MNDO of Dewar.[25] Moreover, almost all of the methods, especially MNDO, converge rapidly toward good minima geometries. Therefore, such a choice represents a sensible procedure to tackle such a difficult problem. We could have used a DFT procedure similar to Mebel et al.,[21] but we have instead built a semiempirical package (AMPAC 6.0) which contains a lot of convenient tools[26] such as powerful self-consistent field convergers, full valence configuration interaction (CI) calculations, efficient optimizers, saddle point and reaction path algorithms, and a global surface investigator. The semiempirical package is an essential feature of our strategy. One more reason is the ease of analysis of the electronic wave function using the molecular orbital language. Such a facility does not exist so far in a DFT description. Obviously, the semiempirical results will be confirmed and improved in a second step by extensive and sophisticated ab initio calculations in order to obtain semiquantitative results. Another reason which could justify the current strategy is its use in the future of the MNDO method as a technique in which the parameters are fitted on ab initio calculations of good qualities as proposed recently by Rossi and Truhlar.[27]

The paper is organized as follows. Section II deals with the theoretical methods employed in this work. In section III, we give the semiempirical results obtained and discuss their implications for the available chemical channels. Section IV contains the ab initio results and their comparison with semiempirical calculations. Comparisons with the most recent results obtained by Mebel et al.[21] are presented in section V. Section VI concerns a qualitative analysis of the wave functions of the structures of some transition states, and in section VII we give our conclusions.

II. Computational Methods

A. Semiempirical Calculations. As explained above, the systematic exploration of the potential energy surfaces has been undertaken using the semiempirical MNDO method[25] coupled to a full CI calculation involving all the determinants constructed with 10 electrons distributed among 10 orbitals. For any four-atom configuration, this method yields the energy values of the singlet and triplet states of interest. Such calculations take into account $C_{10}^5 \times C_{10}^5 = 63\,504$ determinants with a S_z projection equal to 0. AMPAC 6.0 uses a selection scheme to reduce the number of determinants (Δ_i) that are retained for the actual configuration interaction matrix diagonalization. The program first calculates the Epstein−Nesbet[28] energies $\langle \Delta_i H \Delta_i \rangle$ and constructs a target group composed of the ground and a few of the lowest excited determinants. Using the following criterion from perturbation theory for retaining the determinant Δ_k

$$\sum_{i=1}^{n} \left| \frac{\langle \Delta_i | \hat{H} | \Delta_k \rangle}{\langle \Delta_i | \hat{H} | \Delta_i \rangle - \langle \Delta_k | \hat{H} | \Delta_k \rangle} \right| \geq T$$

in which i denotes a determinant of the target group and T a given threshold. At each stage of state selection, all the determinants associated with degenerated Møller−Plesset[29] energies $\langle \Delta_i F \Delta_i \rangle$, F being the Fock operator, are retained. Thus, the procedure fully accounts for spin and space degeneracies.

B. Research and Analysis of the Stationary Points. The search of the stationary points on a potential energy surface (limited here to minima and saddle points, i.e. points characterized by at most one negative eigenvalue of the Hessian matrix) has been conducted using several techniques: the BFGS method,[30] the eigenvector following (EF) algorithm,[31] and the "chain method".[32,26] The first two methods allow stationary points of any kind, i.e. characterized by any number of negative eigenvalues of the Hessian matrix, to be reached, while the third method is only able to determine saddle points but with a great reliability. These three methods are efficient minimizers to determine stationary points only locally. Hence, it is difficult to obtain a complete view of the surface explored. To overcome this difficulty, we have used a nonlocal method based on a simulated annealing technique[33] to visit globally the PES. In this technique, different cost functions can be used such as the potential energy itself or the root mean square gradient norm of the energy. The former choice of cost function leads to the minima only. The latter can give a priori and directly all the stationary points since they correspond to zero minima of the cost function.[34]

Selected geometry inputs and judicious use of various penalty functions—for instance, along the asymptotic valleys to avoid complete separation of the fragments—make a priori the search complete and computationally efficient in an acceptable computing time. Once the saddle points have been found, reaction paths connecting each saddle point to their two related minima can be determined by the exponential predictor corrector (EPC) method[26] which is based on the intrinsic reaction coordinate approach of Fukui et al.[35] and developed by Miller et al.[36] The practical use is presented in section III.

C. Ab Initio Calculations. Ab initio calculations of increasing quality have been performed. These different levels of sophistication involve two large basis sets and advanced methods for a reliable treatment of electronic correlation. As a first step, we have performed UHF/6-31G** calculations of all the structures found within the semiempirical MNDO/CI method. This approach is able to provide a qualitative description of the different bond dissociation energy profiles. These unrestricted Hartree−Fock (UHF) results are not reported here, but were useful for the next step. In a second step, we tried to check our UHF results within a complete active space self-consistent field (CASSCF)[37] method based on the Dunning D95 basis set.[38] The CASSCF approach takes into account the non dynamic correlation, but the bond dissociation is now semi-

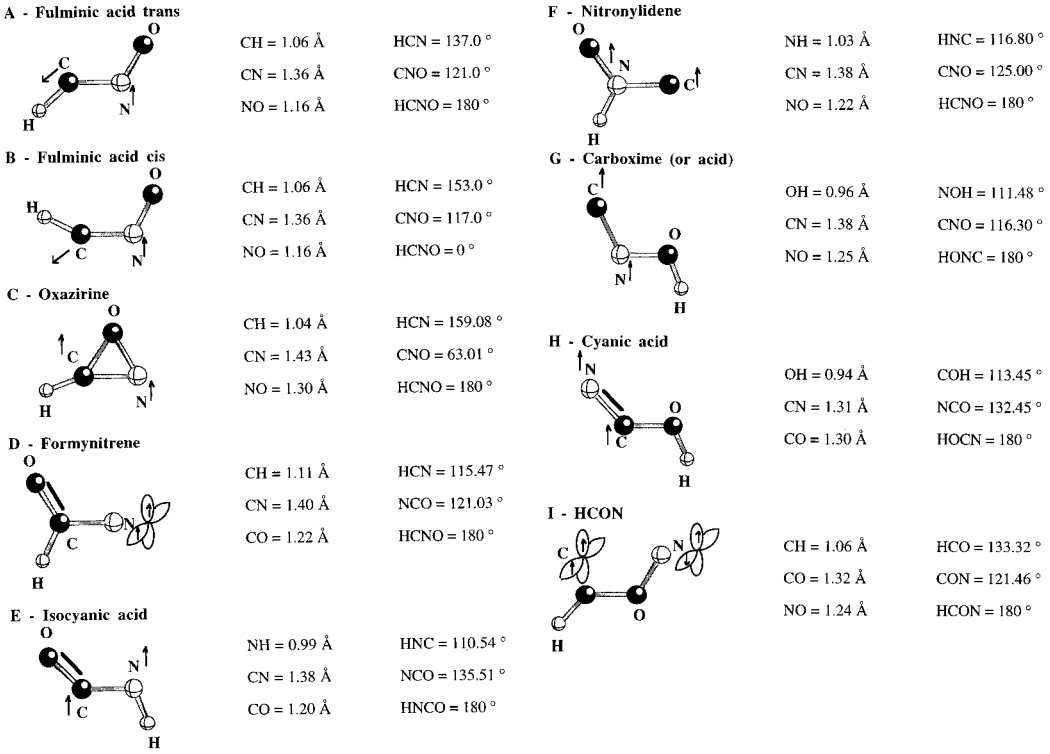

Figure 1. Molecular geometries of the structures associated with the minima found in the triplet surface within the semiempirical MNDO/CI approach. WX is a bond distance, WXY is a planar angle, and WXYZ is a dihedral angle.

quantitatively described.[39] This active space includes 10 orbitals: the nine 2p orbitals for the C, N, and O atoms and the 1s orbital for the H atom. To check the validity of the active space we performed the geometry optimization of one of the saddle points found (labeled 20), employing a full valence complete active space (FVCAS). The results obtained only differ about 0.02 Å for the bond lengths and 2−3° for the angles with respect to the CASSCF optimization. Finally, more precise results have been further obtained by a CASPT2 approach where the dynamic correlation is taken into account at the second-order of the perturbation theory, the zero-order wave function being the CASSCF function. This way to proceed through the CASSCF step gives a valuable reference function for the CASPT2 calculations since a scalable amount of the correlation energy can be obtained through the entire surface to estimate the difference between the CASSCF and the full CI energies.[40] At the CASPT2 level of calculation and for the large basis set used, the bond distances are accurate up to 0.01 Å but the bond energies are underestimated by 3−4 kcal mol^{-1} for each bond formed.[41] Both CASSCF and CASPT2 calculations have been performed using the MOLCAS-3 ab initio package.[42]

III. Results from MNDO/CI

Since all the different stationary points on the singlet surface discovered by Poppinger et al.[17] have been found with the MNDO/CI method, we have assumed that this method is qualitatively reliable and can serve as a guide for the exploration of the topology of the surfaces involved in this reaction. The procedure we have employed to explore a surface is as follows: (i) the Poppinger geometries associated with the stationary points of the singlet surface were used as starting geometries for a local exploration of the lowest triplet surfaces involved in this reaction and (ii) the simulated annealing approach was used to confirm the previous results and make an exhaustive exploration of the relevant surface to search for possible extra stationary points. This strategy is quite justified by the fact that the simulated annealing is not implemented in the ab initio packages.

A potential energy barrier of height 10.06 kcal mol^{-1} (this value corresponds to a real potential energy, not an enthalpy at 0 or 300 K) has been discovered along the linear approach of the reactants in the singlet surface. Conversely, we did not find any barrier on the triplet surface in the entrance channel leading to stable planar triplet *trans*- and *cis*-fulminic acid molecules (**A** and **B** structures defined below). We shall see later that the singlet barrier is drastically reduced to less than 2 kcal/mol at CASPT2 level of calculations (vide infra). Although the singlet surface may play a role in the reaction, the triplet surface, which does not exhibit any barrier at ab initio level and presents a 3-fold degeneracy, is expected to play the major one at 300 K.

Limiting our exploration to the lowest triplet surface (many features are already known on the singlet surface), we have found nine minima and 22 transition states (saddle points) which are expected to play a role in the different channels involved in this reaction. We have used the Poppinger et al.[17] terminology since the triplet and singlet structures both have similar geometrical arrangements. Moreover, most of the semiempirical results concerning the geometries and the status of minima and saddle points found in the first triplet surface are qualitatively conserved when using a more sophisticated ab initio approach.

Figures 1 and 2 show the geometries of the structures corresponding to the nine minima and the 22 saddle points. Table 2 contains the MNDO/CI exoergicity values $\Delta\epsilon_0$ of all the possible channels. The six first channels correspond to the ones investigated experimentally (the available experimental exoergicities are also presented in this table for convenience). As expected, the $\Delta\epsilon_0$ values calculated at the MNDO/CI level are only in a relatively fair agreement with the corresponding experimental exoergicities, $\Delta\epsilon_0$. Table 3 displays the relative enthalpies at 300 K of the stationary points with respect to the enthalpy of the reactants taken as origin (these stationary points are labeled as in Figures 1 and 2). It appears that isocyanic acid (**E**) is the most stable triplet CHNO isomer at this semiempirical level. The nitronylidene (**F**) appears to be the least stable triplet structure by 92.50 kcal mol^{-1} above the stable minimum (**E**). We can summarize these semiempirical results

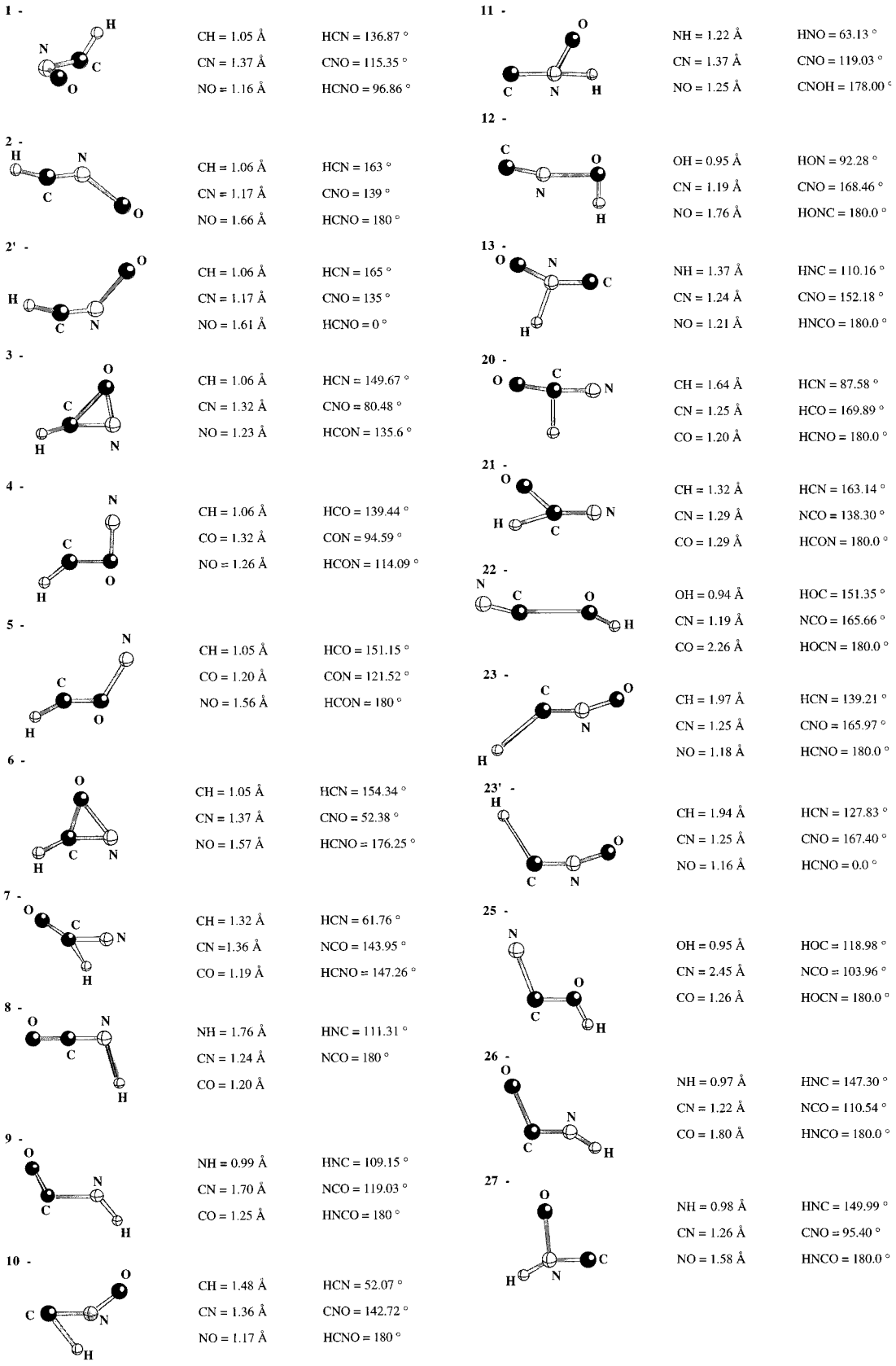

Figure 2. Molecular geometries of the structures associated with the saddle points found in the triplet surface with the semiempirical MNDO/CI approach. Same explanation as in Figure 1.

through the following energy sequence going from the most stable triplet structure to the least stable: **E** > **D** > **H** > **A** > **B** > **C** > **I** > **G** > **F**. A qualitative analysis of the triplet electronic wave functions associated with these minima shows the following results:

(i) *trans*-fulminic acid (**A**) and *cis*-fulminic acid (**B**), oxazirine (**C**), nitronylidene (**F**), and carboxime (**G**) present qualitatively the same electronic distribution concerning the two unpaired electrons. One electron is almost localized on the carbon atom (a fraction of electron evolving between 0.6 and 0.9 e) and the

TABLE 2: Exoergicities ($\Delta\epsilon_0$), Referred to Ground State Reactants CH($X^2\Pi$) + NO($X^2\Pi$)

	experiment[16]		MNDO/CI	
	(eV)	(kcal mol^{-1})	(eV)	(kcal mol^{-1})
$H(^2S) + CNO(X^2\Pi)$	−0.60	−13.84	+0.44	+10.29
$N(^4S) + HCO(X^2A')$	−1.75	−40.36	−0.39	−9.04
$OH(X^2\Pi) + CN(X^2\Sigma^+)$	−2.18	−50.27	−0.77	−17.86
$O(^3P) + HCN(X^1\Sigma^+)$	−3.11	−71.72	−2.17	−50.08
$H(^2S) + NCO(X^2\Pi)$	−3.18	−73.33	−2.57	−59.26
$CO(X^1\Sigma^+) + NH(X^3\Sigma^-)$	−4.86	−112.08	−3.20	−73.84
$O(^3P) + HNC(X^1\Sigma^+)$[44]	−2.07	−47.78	−0.69	−15.83
$C(^3P) + HNO(X^1A')$[45]	+1.35	+31.13	+1.37	+31.55
$C(^3P) + HON(X^1A')$[46]	+3.12	+71.92	+2.73	+62.95
$N(^4S) + HOC(X^2A')$[47]	−0.07	−1.61	+0.69	+15.92

TABLE 3: Relative Enthalpies ΔH_{300} at 300 K, in kcal mol^{-1}, of the Stationary Points (Capital Letter, Minimum; Number, Saddle Point) Found by MNDO/CI Calculations[a]

labels	ΔH_{300}	labels	$\Delta H^{\#}_{300}$	labels	$\Delta H^{\#}_{300}$
A	−59.60	**1**	−55.30	**11**	+69.90
B	−57.00	**2**	+17.60	**12**	+14.55
C	−43.90	**2′**	+19.37	**13**	+33.00
D	−91.70	**3**	−25.10	**20**	−46.40
E	−102.40	**4**	−12.00	**21**	−13.97
F	−9.90	**5**	+26.70	**22**	−11.71
G	−12.90	**6**	−23.10	**23**	+19.77
H	−73.30	**7**	−35.70	**23′**	+23.45
I	−24.20	**8**	−47.90	**25**	+19.12
		9	−59.40	**26**	+17.09
		10	+33.10	**27**	+46.71

[a] The ΔH_{300} quantity of the reactants in their ground electronic state CH($X^2\Pi$) + NO($X^2\Pi$) is taken to be equal to 0.

second one mainly shared between the nitrogen atom (0.6−0.7 e) and the oxygen atom (0.3−0.2 e) with a larger propensity to be on the nitrogen atom.

(ii) Formylnitrene (**D**) displays a slightly polar double CO bond (+0.3 e on C and −0.3 e on O) and two unpaired electrons distributed in two different orbitals ($2p_y$ and $2p_z$) of the nitrogen atom.

(iii) Isocyanic acid (**E**) contains an almost covalent double CO bond and two unpaired electrons, one localized on C and the other on N.

(iv) Cyanic acid (**H**) presents an almost covalent CN double bond and two unpaired electrons on C and N.

(v) The triplet wave function of the HCON structure (**I**) is much more difficult to analyze since, in this case, we have to deal with a four open shell triplet function. This structure can only be described simply by four uncoupled electrons. An electronic pair carrying the spin is kept localized on one atom (C or N) while the other pair is slightly delocalized toward the O atom.

Figure 3a−e displays the qualitative triplet reaction paths connecting the reagents to all the possible products detected experimentally (Table 1). From these results, several general remarks can be made: (i) the semiempirical $\Delta\epsilon_0$ values are ordered in the same sequence as the experimental ones (Table 2), (ii) we can observe that all the semiempirical $\Delta\epsilon_0$ values are systematically greater than the experimental $\Delta\epsilon_0$ values by roughly 20−30 kcal mol^{-1}, (iii) for all these paths, the first step is the formation of the fulminic acid in a trans (**A**) or cis (**B**) conformation, which is readily formed by long range interaction between CH and NO (mainly a dipole-dipole interaction).[23b]

(i) Figure 3a shows the reaction paths connecting the reactants CH + NO to the products HCN + O. One intermediate appears, namely the planar *trans*-fulminic acid (**A**) or the planar *cis*-fulminic acid (**B**). Along this path, **A** can undergo a rearrangement into its **B** isomer through a saddle point labeled **1** characterized by a structure in which the C−H bond is out of the CNO plane, so by a rotation of the C−H bond around the C−N bond we form the planar trans structure (**A**) or the planar cis structure (**B**). The system can then evolve toward the products from the *trans*-fulminic acid (**A**) through a saddle point labeled **2** associated with a trans structure or from the *cis*-fulminic acid (**B**) via a saddle point labeled **2′** with a cis structure. Both saddle points correspond to a structure in which the N−O bond is substantially elongated (1.60 Å) with respect to the N−O equilibrium distance (1.16 Å) in **A** and **B**. These barriers, **2** and **2′**, seem to be rather high (19.4 kcal mol^{-1} and 17.6 kcal mol^{-1} height, respectively) and this could be a priori an efficient kinetic obstacle against the formation of the products HCN + O, a result which seems to be in contradiction with the observation of Lambrecht et al.[13] However, these barriers are drastically decreased at the ab initio level as discussed in section IV.

(ii) Figure 3b deals with the reaction path connecting the reactants to the products HCO + N. Three intermediates are present: planar *trans*-fulminic acid (**A**), planar oxazirine (**C**) and a planar trans structure HCON (**I**). Evolution from **A** to **C** occurs via saddle point **3** characterized by a decrease of the C−O bond with respect to **A** (2.20 Å in **A**, 1.68 Å in **3**, and 1.43 Å in **C**) and a slight out of plane motion of the H atom. Oxazirine (**C**) can rearrange into the stable structure **I** via barrier **4** by the stretching of the C−N bond (1.43 Å in **C**, 1.88 Å in 4, and 2.23 Å in **I**). The passage from **I** to products HCO + N through a barrier labeled 5 involves O−N bond cleavage. It is clear that this pathway shows a saddle point (**5**) energetically higher than the reactants. Moreover, it displays more rearrangements than the previous one (Figure 3a), and each chemical step reduces the rate constant of the channel of interest by a quantity always smaller than 1. This fact is related to the forward and the backward trajectory fluxes through the phase space region of the intermediate stable structure.[43] These arguments make the formation of products HCO + N less likely than that of HCN + O.

(iii) Figure 3c describes the triplet pathways connecting the reactants to the products NCO + H and CO + NH. Three or four intermediates have to be taken into account (**A**, **C**, **D**, and **E**), the first two being the same as in the previous reaction path (Figure 3b, formations of *trans*-fulminic acid (**A**) and oxazirine (**C**)). Oxazirine (**C**) evolves into planar formylnitrene (**D**) through a saddle point (**6**) by progressive extension of the N−O bond (1.30 Å in **C**, 1.57 Å in **6**, and 2.28 Å in **D**), while the C−H bond undergoes a weak out of plane motion. From the planar structure **D**, we can evolve directly (dashed line) toward the products NCO + H over a barrier (saddle point labeled **20**) associated with a structure in which the C−H bond is largely elongated (1.64 Å). The formylnitrene (**D**) can also rearrange into isocyanic acid (**E**) via barrier **7** corresponding to a H-bridged structure over the C−N bond. Formation of products CO + NH from isocyanic acid (**E**) requires the passage over saddle point **9**. The products NCO + H can also be reached from isocyanic acid (**E**) via a barrier (**8**) by stretching of the N−H bond (1.76 Å). Although all the barriers found are lower than the energy of the reagents, the numerous molecular rearrangements involved to reach both products are unfavorable for the formation of these products (see last comment in the preceding paragraph ii).

(iv) Figure 3d.α,d.β shows that two triplet pathways are to be considered for the formation of the products CN + OH. In the first pathway proposed (Figure 3d.α), three intermediates are found: **A**, **F**, and **G**. *trans*-Fulminic acid (**A**) transforms into planar nitronylidene (**F**) via a high barrier labeled **10** corresponding to a planar structure in which the H atom is

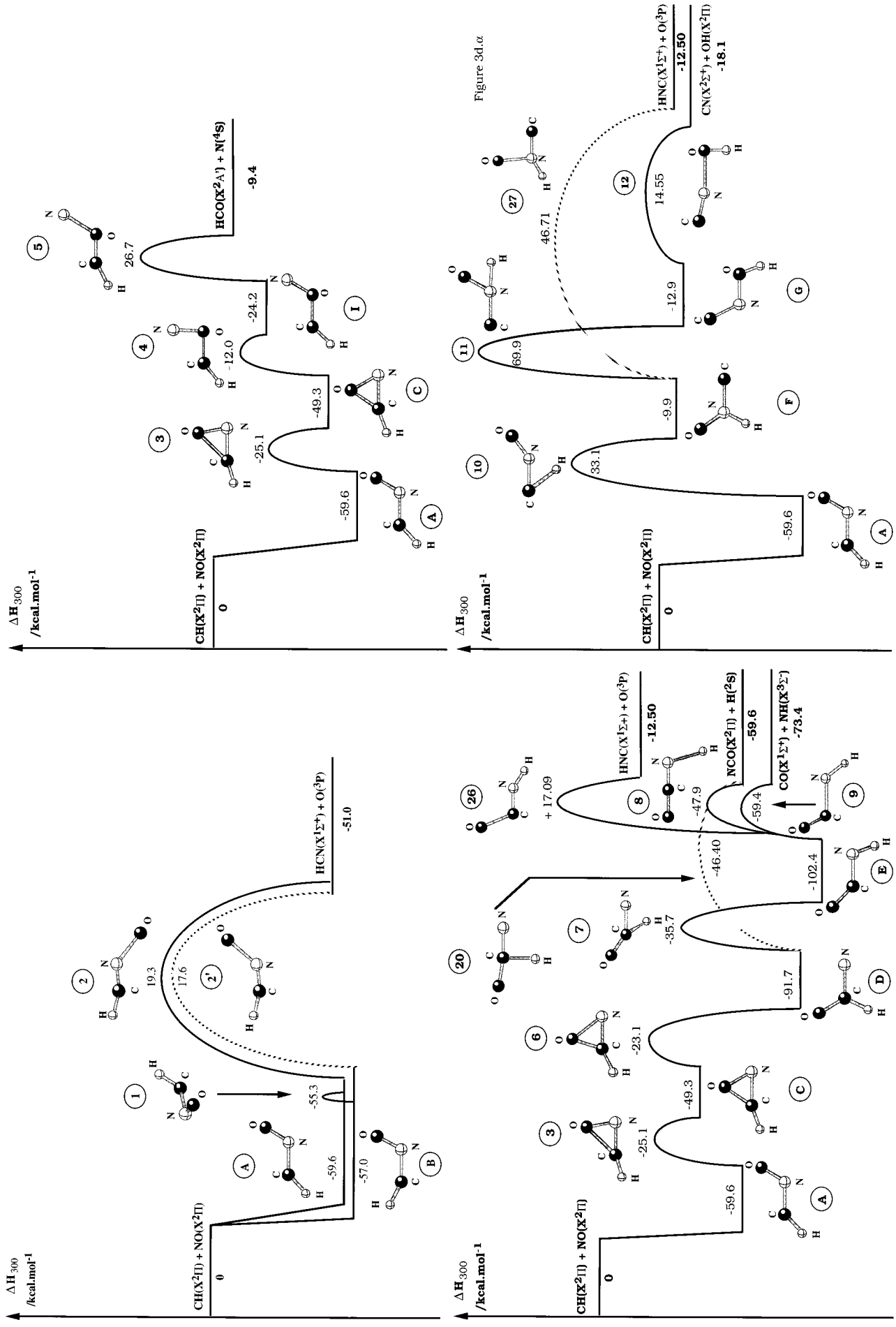
ΔH300 /kcal.mol-1
CH(X2Π) + NO(X2Π)
0
-59.6
-25.1
-49.3
-12.0
-24.2
26.7
HCO(X2A') + N(4S)
-9.4
A
C
I
ΔH300 /kcal.mol-1
CH(X2Π) + NO(X2Π)
0
-59.6
33.1
-9.9
69.9
-12.9
46.71
14.55
HNC(X1Σ+) + O(3P)
-12.50
CN(X2Σ+) + OH(X2Π)
-18.1
A
F
G
ΔH300 /kcal.mol-1
CH(X2Π) + NO(X2Π)
0
-59.6
-55.3
-57.0
19.3
17.6
HCN(X1Σ+) + O(3P)
-51.0
A
B
ΔH300 /kcal.mol-1
CH(X2Π) + NO(X2Π)
0
-59.6
-25.1
-49.3
-23.1
-91.7
-35.7
-46.40
+ 17.09
-47.9
HNC(X1Σ+) + O(3P)
-12.50
-59.4
NCO(X2Π) + H(2S)
-59.6
-102.4
CO(X1Σ+) + NH(X3Σ-)
-73.4
A
C
D
E

Figure 3d.*a*

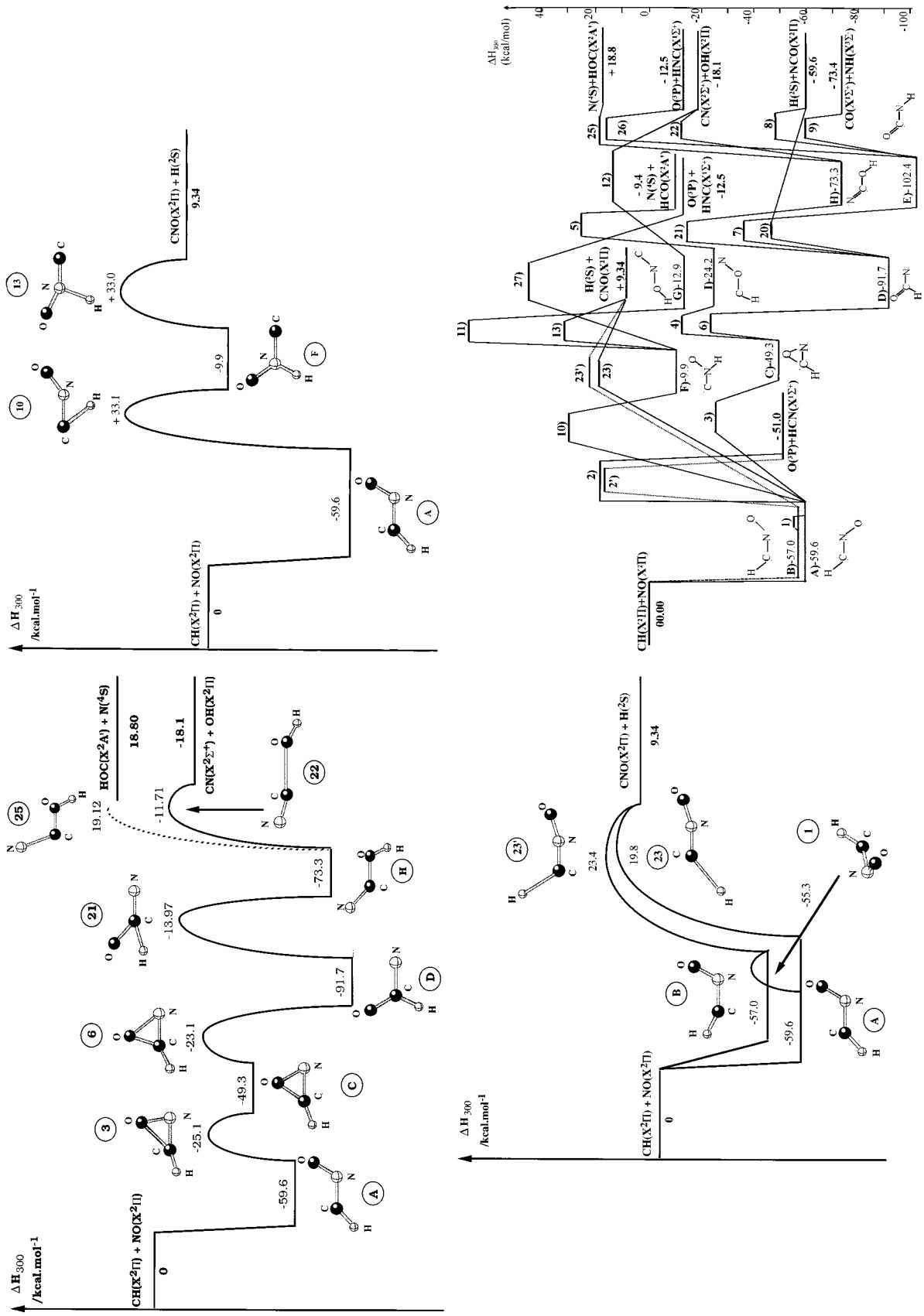

Figure 3. Triplet reaction paths at the MNDO/CI level connecting the reagents CH($X^2\Pi$) and NO($X^2\Pi$) to the different product channels involved in the reaction. The enthalpies ΔH_{300} at 300 K are in kcal mol^{-1}. Capital letters in the labels correspond to minima and the numbers to saddle points. (Previous page: a, top left; b, top right; c, bottom left; d.α, bottom right. This page: d.β, top left; e.α, top right; e.β, bottom left.) Potential energy profiles of the HCNO system calculated at the semiempirical level (MNDO/CI). (This page: f, bottom right.)

bridged over the C−N bond. Then, formation of planar carboxime (**G**) from nitronylidene (**F**) requires a H transfer from the N atom to the O atom via a very high barrier labeled 11 associated with an almost planar structure. The passage from the carboxime (**G**) to the products CN + OH through a barrier labeled **12** involves N−O bond breaking, the four atoms staying in a plane through this process. The second pathway leading to the products CN + OH involves four intermediates (Figure

3d.β), the first three being the same as in the reaction path of Figure 3c (formations of *trans*-fulminic acid (**A**), oxazirine (**C**), and formylnitrene (**D**)). The next step is the migration of the hydrogen atom from the carbon atom in structure **D** to the oxygen atom in the cyanic acid **H** via a saddle point (**21**) characterized by a drastic decrease of the HCO angle (123.32° in **D**, 58.56° in **21**, and 27.24° in **H**). To reach the products CN + OH from structure **H**, the system has to pass over a barrier (**22**) in which the C−O bond distance is substantially elongated (2.26 Å in **22** compared to 1.30 Å in **H**). In the first reaction path (Figure 3d.α), the existence of very high barriers (**10** and **11**) makes the formation of CN and OH radicals highly unlikely. The second path (Figure 3d.β) takes into account lower barriers, but involves a fairly large number of rearrangements to obtain the products and may suggest that these products can only be formed in small amounts.

(v) Figure 3e.α,d.β deal with the two reaction paths leading to the formation of the less exoergic products CNO + H. In the first path found (Figure 3e.α), the two steps (formations of the *trans*-fulminic acid (**A**) and the nitronylidene (**F**)) are common with the previous path leading to CN + OH (Figure 3d.α). Nitronylidene (**F**) then gives the separated fragments CNO + H by H−N bond breaking and alignment of the three atoms C, N, and O in the ground electronic state $X^2\Pi$ of CNO. The products CNO + H can also be formed directly by the cleavage of the C−H bond in *trans*- (**A**) or *cis*-fulminic acid (B) via barriers labeled **23** and **23′**, respectively (Figure 3e.β). It is clear that neither of these two reaction paths, shown in parts 3e.α and 3e.β of Figure 3, is favorable to the formation of the products CNO + H since the pathways shown in parts 3e.α and 3e.β of Figure 3 involve rather high barriers (saddle points **10**, **13**, **23**, and **23′**) with respect to the energy of the reactants.

By a systematic census of all the possible arrangements between the four atoms, we can also suggest the formation of some other products like HOC + N, HNC + O, HON + C, and HNO + C that have not been experimentally considered so far and try to find some paths connecting these products to the reactants. The experimental $\Delta\epsilon_0$ values available in the literature for the HNC + O,[44] HNO + C[45] and HON + C[46] product channels are presented in Table 2. No experimental $\Delta\epsilon_0$ value is available for the HOC minimum, but theoretical work[47] reports a HOC structure 1.68 eV (38.7 kcal mol^{-1}) above its isomer HCO. The HNO + C and HON + C product channels are endothermic and thus thermodynamically inaccessible at 300 K. Using some "chemical intuition" coupled to simulated annealing technique, we can imagine the sequence of possible rearrangements connecting the reactants CH + NO to the products HNC + O and HOC + N. Direct formation of products HNC + O can be envisaged by C−O bond cleavage in the stable structure HNCO (structure **E**) and by N−O bond breaking in the star-shaped structure (**F**). Related to the formation of HOC + N, we have to consider the rupture of the C−N bond in HOCN (structure **H**) and the rupture of the N−O bond in a hypothetical star-shaped structure (**J**) in which the oxygen atom occupies the center of the star. Following this idea, we found that the exothermic products HNC + O can be effectively reached from the stable isocyanic acid (**E**) occurring in the reaction path of Figure 3c via a barrier labeled **26** (17.09 kcal mol^{-1}) and characterized by a large stretching of the C−O bond (1.80 Å in **26** and 1.20 Å in **E**). The height of the barrier **26** and the large number of molecular rearrangements are unfavorable for the formation for HNC + O compared to that for its isomer HCN + O (which can be directly formed from *trans*- (**A**) and *cis*-fulminic acid (**B**) Figure 3a). It turns out that HNC + O can be formed from nitronylidene (**F**) involved in the pathway displayed in Figure 3d.α. The passage from the nitronylidene (**F**) to HNC + O through a very high barrier labeled **27** (46.71 kcal mol^{-1}) involves breaking of the N−O bond. Thus, the full reaction path presents two very high barriers (**10** and **27**) which make the formation of HNC + O very unlikely. Moreover HNC is known to quickly isomerize to HCN. Concerning the formation of HOC + N, the cyanic acid (**H**) of Figure 3d.β evolves toward HOC + N through a rather high barrier labeled **25** (19.12 kcal mol^{-1}) corresponding to a structure in which the C−N bond is largely elongated (2.25 Å in **25** and 1.31 Å in **H**). The four first intermediates **A**, **C**, **D**, and **H** of this reaction path are common with the formation of CN + OH (Figure 3d.β). The numerous molecular rearrangements encountered along this path and the height of the barrier **25** could be an efficient kinetic obstacle against the formation of the products HOC + N. The hypothetical structure (**J**) suggested above (the oxygen atom being at the center of the star shape) has been found to be 60.99 kcal/mol above the reactants, a result which totally prevents the formation of HOC + N from this way. In conclusion, the formation of HOC + N and HNC + N as major products of the reaction CH + NO is highly unprobable due to the high barriers (saddle points **25** and **26**) and the large number of chemical rearrangements encountered along these paths. Among the six open channels explored at semiempirical level (Table 1), it transpires that the path leading to the exothermic formation of HCN + O (Figure 3a) is the one with the smallest number of molecular rearrangements but presenting rather high barriers. The paths leading to the very exothermic formation of NCO + H and CO + NH (Figure 3c) seem to be the most kinetically favorable channels. These qualitative results are only in fair agreement with the experimental findings mentioned in section II, but we might expect that most of the barrier heights found in this study will be substantially decreased when using a sophisticated ab initio treatment.

All these MNDO/CI results are collected in Figure 3f where comparison of the various paths is made easier.

TABLE 4: Exoergicities ($\Delta\epsilon_0$), in eV, Referred to Ground State Reactants CH($X^2\Pi$) + NO($X^2\Pi$)

	expt[16]	CASSCF/D95	CASPT2/D95
$H(^2S) + CNO(X^2\Pi)$	−0.60	+0.32	−0.56
$N(^4S) + HCO(X^2A')$	−1.75	−2.57	−2.58
$OH(X^2\Pi) + CN(X^2\Sigma^+)$	−2.18	−2.32[a] (−1.20)	−2.23[a] (−2.14)
$O(^3P) + HCN(X^1\Sigma^+)$	−3.11	−3.38	−3.54
$H(^2S) + NCO(X^2\Pi)$	−3.18	−2.46	−3.38
$CO(X^1\Sigma^+) + NH(X^3\Sigma^-)$	−4.86	−5.06	−4.91
$O(^3P) + HNC(X^1\Sigma^+)$[44]	−2.07	−3.37	−3.03
$C(^3P) + HNO(X^1A')$[45]	+1.35	+1.55	+1.10
$C(^3P) + HON(X^1A')$[46]	+3.12	+3.83	+3.47
$N(^4S) + HOC(X^2A')$[47]	−0.07	−0.61	−0.66

[a] To get a correct description of $CN(X^2\Sigma^+)$, we have used an extended active space in the MCSCF CAS approach where the 3s atomic orbitals are included. The values in parentheses are obtained without this extended active space.

IV. Ab Initio Results

Table 4 contains the six channel exoergicities referred to ground state reactants obtained at CASSCF and CASPT2 levels of calculation. Both methods lead to acceptable results. As expected, CASPT2 calculations lead to values in better agreement with experiment than CASSCF, the least good agreement concerning the channel leading to HCO + N. This is probably due to a much better description of $N(^4S)$ involving three uncoupled electrons than that of the HCO system. Conversely, $CN(X^2\Sigma^+)$ is incorrectly described with the active space mentioned in section II.C (see value in parentheses in Table 4). Therefore, a larger active space should be taken into account to improve the CASSCF level of calculation on CN (3s atomic

TABLE 5: Relative Enthalpies ΔH_{300} at 300 K (in kcal mol^{-1}) of the Stationary Points (Capital Letter, Minimum; Number, Saddle Point) Deduced from the CASPT2/D95 Approach[a]

labels	ΔH°_{300}	labels	$\Delta H^{\#}_{300}$	labels	$\Delta H^{\#}_{300}$
A	−63.59	**1**	−46.84	**11**	+9.46
B	−62.63	**2**	−50.12	**12**	−29.56
C	−54.70	**2′**	−62.21	**13**	+5.05
D	−118.46	**3**	−54.48	**20**	−77.99
E	−115.06	**4**	−7.51	**21**	−84.72
F	−46.36	**5**	−30.60	**22**	−54.21
G	−30.88	**6**	−43.78	**23**	−20.34
H	−86.01	**7**	−78.63	**23′**	−19.83
I	−35.48	**8**	−65.23	**25**	no barrier
		9	−109.14	**26**	−67.03
		10	−16.59	**27**	−43.48

[a] Same origin of the energies as in Table 3. These values are the sum of the CASPT2/D95 values to the potential energy, the zero-point energy levels, and the thermal enthalpies at 300 K.

orbitals are included). Moreover, the use of this new active space for CN does not significantly change the energies of the NO and CO systems.

The first important result arising from these ab initio studies is the lack of barrier along the entrance channel leading to the trans (**A**) and cis (**B**) configurations of fulminic acid in the lowest triplet state surface. On the other hand, we still find a potential energy barrier along the singlet surface, but much lower than at the semiempirical level (1.20 kcal mol^{-1} instead of 10.06 kcal mol^{-1}).

Whatever the level of ab initio calculations, we have found analogous geometries for almost all the minima and saddle points already discovered at MNDO/CI level, and thus the ab initio and semiempirical reaction paths can be considered to be roughly topologically equivalent. This comparison proves the reliability of the semiempirical approach at a qualitative level of description. Table 5 contains the relative CASPT2 enthalpies at 300 K of the stationary points with respect to the reagents. Differences with semiempirical values are worth pointing out: (a) formylnitrene (**D**), rather than isocyanic acid (**E**), appears to be the most stable CHNO isomer, but the CASPT2 energy difference is small (3 kcal mol^{-1}) and (b) the less stable structure is now carboxime (**G**) instead of nitronylidene (**F**). At the CASPT2 level of calculation, the list of relative stabilities of these minima is now the following: **D** > **E** > **H** > **A** > **B** > **C** > **F** > **I** > **G** (being **E** > **D** > **H** > **A** > **B** > **C** > **I** > **G** > **F** at MNDO/CI level).

Figure 4a−e shows the different paths associated with the six exoergic channels presented in Table 1. The same order of presentation as in section III has been conserved. In order to compare with MNDO/CI results, we have calculated the thermal enthalpies at 300 K from the ab initio potential energy values, the zero-point energy level, and the thermal energies between 0 and 300 K.

A general comment concerns the geometrical changes observed at CASSCF level with respect to MNDO/CI level (no geometry optimization has been performed at CASPT2 level). We mainly notice (Table 6) that all the structures associated with barriers present longer bond lengths than those found from a semiempirical description. Concerning the angles, they are, on average, smaller than the parent angles defined in Figure 2.

(i) Figure 4a shows the pathways leading to the products HCN + O. The important result is now the quasi-disappearance of barriers 2 and 2′. The formation of the products HCN + O appears now to be mainly direct. Thus, this channel is very likely at this level of calculation: a result in much better agreement with experiment than previously found.

(ii) Figure 4b deals with the reaction path leading to HCO + N. All the structures (**A**, **C**, **I**, **3**, **4**, and **5**) found at the MNDO/CI level have been confirmed with the two ab initio approaches but, as expected, noticeable energy differences occur: (i) Barrier **3** is largely reduced, almost vanishing on the side of the **C** intermediate formation, and (ii) barrier **4** is now the main potential obstacle on the route to the formation of HCO + N products since barrier **5** is also drastically reduced. Conversely to the reaction path shown in Figure 3b, the formation of HCO + N now becomes feasible since barrier **4** is below the energy of the reactants. Hence, this channel is likely but to a lesser extent than the HCN + O channel, a result in close qualitative agreement with experimental findings.

(iii) Figure 4c is related to the formation of NCO + H and CO + NH. All the structures previously found (**D**, **E**, **6**, **7**, **8**, **9**, and **20**) are obtained again at the CASPT2 level of calculation but with a much lower enthalpy (relative to the reactants) than at the semiempirical level. This result makes these two pathways thermodynamically more favorable than they were previously (MNDO/CI results), although numerous rearrangements are still a factor reducing the rate constants of these channels (see the discussion in section III). Nevertheless, the presence of deep wells associated with the intermediates **D** and **E** can be a trap for the system especially if the pressure increases. Concerning the competition between the two paths leading to the formation of NCO + H from intermediate **D**, we note that in both descriptions the direct formation of NCO + H from **D** is more probable than the passage via intermediate **E**. In fact at the MNDO/CI level, barrier **7** is the relevant obstacle with respect to barrier **20** while at the CASPT2 level barrier **8** plays this role.

(iv) Figure 4d.α,d.β concerns the formation of CN + OH. In the first pathway (Figure 4d.α) the three barriers, **10**, **11**, and **12**, found at the semiempirical level (Figure 3d.α) have significantly decreased in energy. Barrier **12** drastically decreases (we present the CASSCF value for this barrier as we have some difficulties to locate it), but barrier **11** still remains above the energy of the reactants, which makes this path unlikely. The second pathway (Figure 4d.β) exhibits a drastic reduction of barrier heights **21** and **22** (barriers **3** and **6** having already been encountered). At the same time, important changes in the geometry of the structures corresponding to these saddle points (**21** and **22**) appear. In the CASSCF structure of barrier **21**, the hydrogen atom can be considered as bound to the oxygen atom since the O−H distance is 0.97 Å. This distance was larger in the MNDO structure (1.28 Å), and the H atom was still considered to be linked to the carbon atom. These results (CASSCF and MNDO/CI) are consistent with the Hammond postulate which suggest that barrier **21** is energetically much closer to intermediate **H** at the CASPT2 level than at the MNDO/CI level. The main changes occurring in the geometry of the saddle point (**22**) come from the substantial reduction of the C−O bond distance and the large decrease of the HOC and NCO angles (Table 6 compared to Figure 2). This pathway now presents very low barriers but still involves a large number of molecular rearrangements. Its participation in the reaction remains questionable. Moreover, the **D** well is present and could lead directly to dissociation into NCO + H (Figure 4c).

(v) Figure 4e.α,e.β shows the two possible reaction paths leading to the less exoergic products CNO + H. In the first path (Figure 4e.α), all the semiempirical structures have been confirmed in CASSCF and CASPT2 calculations. Note that barrier **13** still remains higher than the energy of the reactants so that the products CNO + H cannot be easily reached from the nitronylidene (**F**). In the second possible reaction path (Figure 4e.β), the large reduction of the relative enthalpies of the barriers **23** and **23′** makes the formation of CNO + H favorable, although fulminic acids **A** and **B** can be stabilized

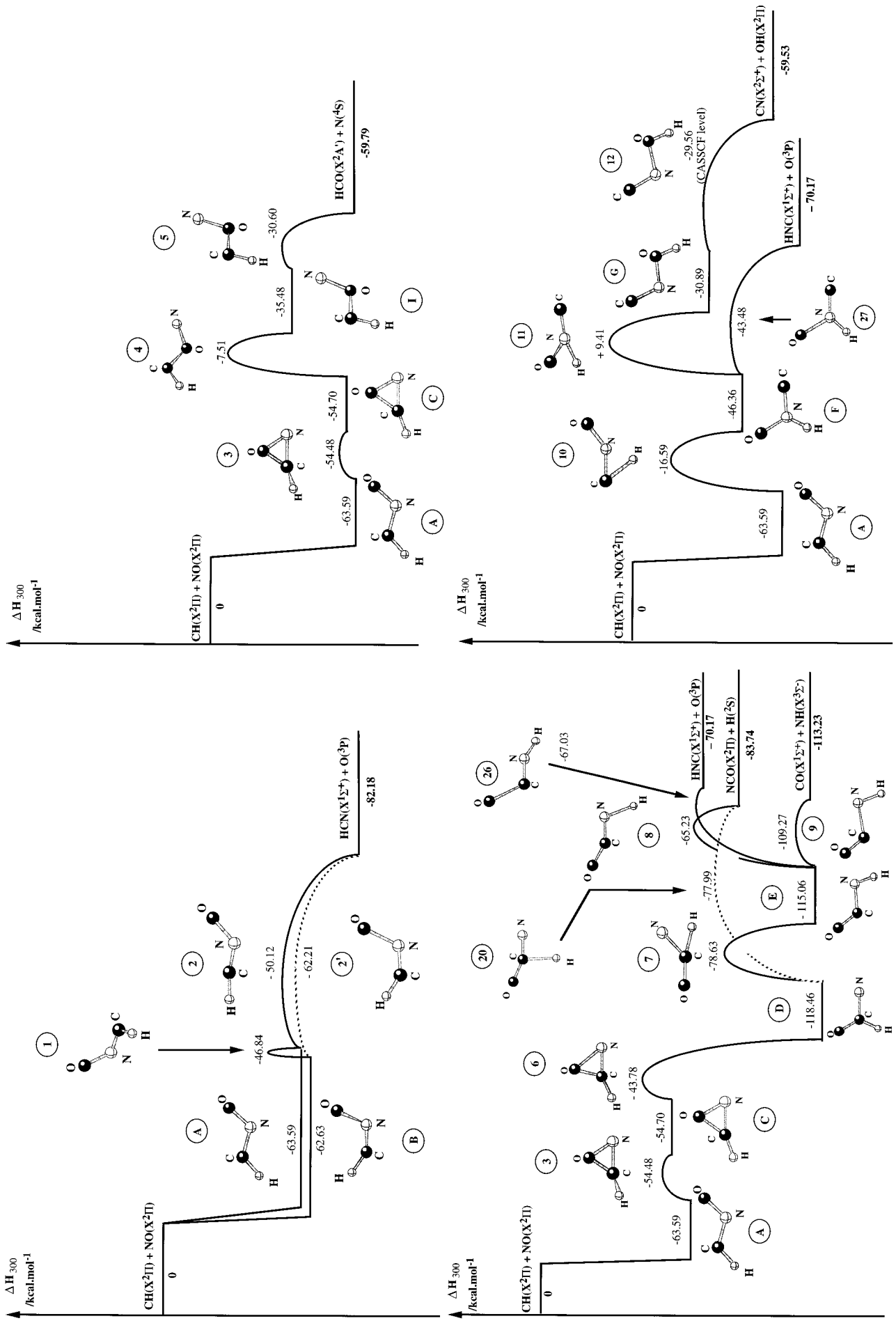
ΔH 300 /kcal.mol-1
CH(X2Π) + NO(X2Π)
0
-63.59
-54.48
-54.70
-7.51
-35.48
-30.60
HCO(X2A') + N(4S)
-59.79
-46.84
-50.12
-62.21
-62.63
HCN(X1Σ+) + O(3P)
-82.18
+9.41
-16.59
-46.36
-43.48
-30.89
-29.56
(CASSCF level)
HNC(X1Σ+) + O(3P)
- 70.17
CN(X2Σ+) + OH(X2Π)
-59.53
-67.03
-65.23
-77.99
-78.63
NCO(X2Π) + H(2S)
-83.74
-109.27
- 115.06
CO(X1Σ+) + NH(X3Σ-)
-113.23
-43.78
-118.46

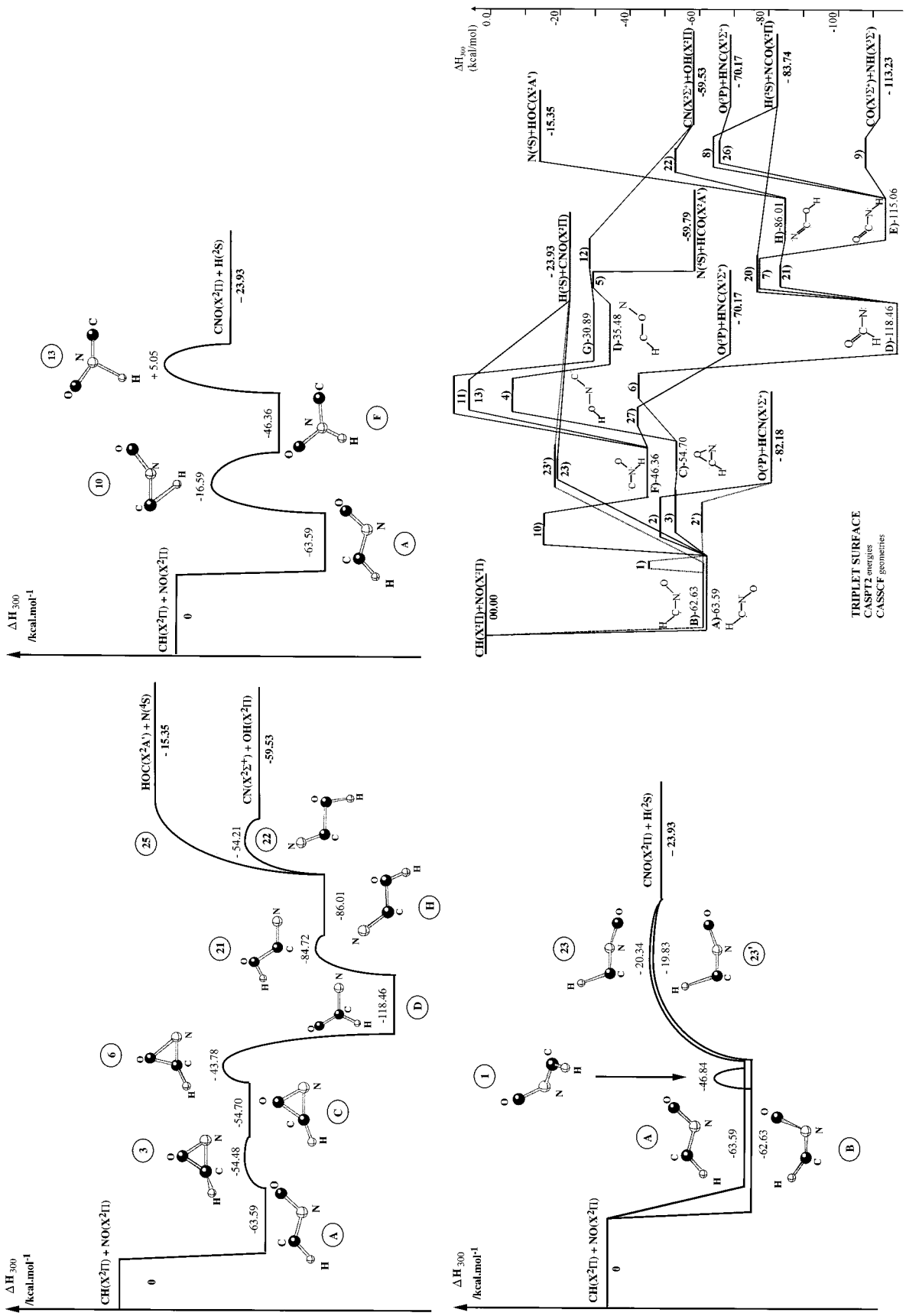

Figure 4. Triplet reaction paths at the CASPT2/D95 level connecting the reagents CH($X^2\Pi$) and NO($X^2\Pi$) to the different product channels involved in the reaction. The enthalpies ΔH_{300} at 300 K are in kcal mol^{-1}. (Previous page: a, top left; b, top right; c, bottom left; d.α, bottom right. This page: d.β, top left; e.α, top right; e.β, bottom left.) Potential energy profiles of the HCNO system calculated at the ab initio level (CASPT2/D95). (This page: f, bottom right.)

by increasing pressure. We note a lessening of the C−H bond distance in the CASSCF geometries of structures **23** and **23′** with respect to the MNDO/CI values (Table 6 compared to Figure 2).

To complete the study of this reaction, we have performed CASSCF and CASPT2 calculations on the two last possible product channels, HNC + O and HOC + N. The saddle points **26** and **27** found at the semiempirical level were confirmed at

TABLE 6: Geometries of the Molecular Structures Associated with the Stationary Points Found by the CASSCF/D95 Approach[a]

labels	CH	CN	NO	HCN	CNO	HCNO
A	1.08	1.36	1.28	122.27	115.78	180
B	1.03	1.26	1.29	127.72	109.25	0
C	1.06	1.44	1.46	158.32	56.58	180

labels	XH	CN	CO	planar angles	NCO	dihedral angles
D	CH = 1.09	1.43	1.23	HCN = 115.47	120.97	HCNO = 180
E	NH = 1.01	1.46	1.20	HNC = 106.73	124.88	HNCO = 180
H	OH = 0.95	1.31	1.36	COH = 109.14	123.26	HOCN = 180
I	CH = 1.10	NO = 1.40	1.34	HCO = 100.90	CON = 112.20	HCON = 180

labels	XH	CN	NO	planar angles	CNO	dihedral angles
F	NH = 1.0	1.34	1.34	HNC = 123.34	122.70	HNCO = 180.0
G	OH = 0.99	1.36	1.37	HON = 105.18	110.40	HONC = 180.0

labels	CH	CN	NO	HCN	CNO	dihedral angles
1	1.07	1.42	1.26	130.60	113.13	HCNO = 92.35
2	1.06	1.23	1.49	177.16	116.40	HCNO = 180.0
2′	1.07	1.23	1.55	144.22	116.90	HCNO = 0.0
23	1.60	1.23	1.24	108.12	162.55	HCNO = 180.0
23′	1.70	1.23	1.25	108.30	158.33	HCNO = 0.0
3	1.05	1.44	1.45	166.01	55.55	HCON = 177.0

labels	CH	CO	NO	HCO	CON	dihedral angles
4	1.10	1.41	1.36	102.90	117.48	HCON = 91.26
5	1.10	1.27	1.40	104.22	108.52	HCON = 180.0

labels	NH	CN	CO	HNC	NCO	HNCO
7	CH = 1.30	1.40	1.21	57.19	134.55	134.8
8	1.49	1.28	1.21	110.25	150.67	180.0
9	1.02	1.76	1.17	101.24	121.03	180.0

labels	NH	CN	NO	HNC	CNO	dihedral angles
10	1.24	1.36	1.31	60.55	121.59	HCNO = 180.0
13	1.50	1.24	1.32	117.8	143.29	HNCO = 180.0
26	0.99	1.21	CO = 1.81	148.02	NCO = 117.30	HNCO = 180.0
27	1.02	1.27	1.55	132.40	121.9	HNCO = 180.0
11	1.19	1.34	1.49	HON = 50.77	121.26	HONC = 180.0
12	OH = 0.98	1.32	1.50	HON = 99.69	109.38	HONC = 180.0

labels	XH	CN	CO	HCN	NCO	dihedral angles
6	CH = 1.06	1.42	1.34	147.99	74.97	HCNO = 180.0
20	CH = 1.72	1.26	1.23	99.22	157.20	HNCO = 180.0
21	OH = 0.97	1.31	1.37	HOC = 107.48	122.40	NCOH = 180.0
22	OH = 0.98	1.23	1.85	HOC = 100.23	111.98	HOCN = 180.0

[a] Bond distances XY in angstroms and planar angles XYZ in degrees.

these ab initio level of calculation (Table 5 and Figure 4c,d.α). The heights of these two barriers have drastically decreased in energy, but the barrier associated with the saddle point **26** remains lower than the barrier **27**. Consequently, the products HNC + O are preferably reached from the stable isocyanic acid (**E**) via the barrier **26** than from nitronilydene (**F**) through the barrier **27**. However globally, these products are unlikely in this reaction due to the large number of rearrangements occurring along the reaction path. The direct formation of its isomer HCN from the fulminic acid (**A** or **B**) is much more probable. Concerning the formation of HOC + N, the barrier associated with the saddle point **25** has disappeared in the CASSCF calculation, so that these products are directly reached from the cyanic acid (**H**) (Figure 4d.β). This direct process makes the formation of HOC + N more likely than that of CN + OH (Figure 4d.β), but HOC + N still highly unprobable as major product channel because this product channel is the least exothermic. All the CASPT2 results are gathered in Figure 4f.

V. Comparisons with the Recent Study of Mebel et al.

Our results compare with those of Mebel and co-workers,[21] being globally in a good agreement. Nevertheless, it is interesting to point out the major differences. We find different results concerning the nature of some of the intermediates and critical points.

First of all, a tiny barrier has been found along the entrance channel in the singlet surface at CASPT2/D95 level whereas no barrier has been found at DFT/B3LYP/6-311G** level. Concerning the triplet fulminic acid (labeled **3** in their paper), we found two planar minima, trans (**A**) and cis (**B**), and a nonplanar transition state (1). Mebel et al. found a planar *trans*-fulminic acid transition state, a nonplanar trans minimum and a planar cis minimum. The same comment can be made about the isocyanic (**E**) and the cyanic acid (**H**) in our work (labeled **1** and **2** in the paper of Mebel et al.). Moreover, they did not find the carboxime (**G**) minimum. The comparison between the transition states of both studies reveals some differences in the geometries and the relative energies. Concerning the geometries, we found at the CASSCF level that most of the structures associated with barriers present shorter bond lengths and smaller angles than those found in B3LYP calculations. Moreover, all the geometries of transition states leading to an asymptotic product channel correspond to a value of the reaction coordinate (which is mainly a bond distance in all the cases)

shorter at the CASSCF level than at the B3LYP level (for example: in structure **2′** (TS3O1) the N−O bond is 1.55 Å in CASSCF and 1.61 Å at B3LYP level; in structure 8 (TS1H1), NH = 1.49 Å at CASSCF level and NH = 1.55 Å at B3LYP level; in structure **9** (TS1D2), CN = 1.76 Å in CASSCF calculations and CN = 1.97 Å in B3LYP calculations). Good agreement is obtained from both approaches on the dihedral angles of the structures of the saddle points found. Nevertheless, two of these structures (labeled **10** and **21** in our paper) present a nonplanar shape from the study of Mebel et al. (TS38 and TS27) and a planar one from our work.

Finally, we note several differences concerning the possible reaction paths involved in this process. First of all, Mebel et al. do not report the existence of barriers **1**, **2**, **3**, **6**, **11**, **12**, and **23** although they do mention other transition states such as TS12 (which corresponds to a barrier between intermediates **E** and **H**), TS18 (between **E** and **F**), TS2H1 (between **H** and the products NCO + H), and TS7O1 (between **D** and HCN + O). In fact, we found similar structures, but, since our main goal is to determine the more probable products, we have reported here only the structures which are expected to play a role in the reaction. As an example, TS7O1 does not seem to be a relevant transition state for the formation of HCN + O since intermediates **A** or **B** are linked directly to these products. In the same way, the products NCO + H can be reached directly from the intermediate **D**. Transition state TS2H1 does not play any role. These different pathways presented in Figure 4f can be easily compared with Figure 12 from the work of Mebel et al.[21]

Besides a simple enumeration of the differences between our ab initio results and the DFT results of Mebel et al., it could be valuable to mention some interpretations of these differences. Such a task looks rather difficult to achieve so far, and it would be even harder to argue for any system which method is valuable and which method is wrong. Nevertheless, some general comments can be formulated about DFT calculations. It is admitted that exchange−correlation functionals are in general well adapted to get reliable geometries and energies of stable systems, i.e. systems associated with a well in a potential energy surface. Moreover, the vibrational frequencies are well reproduced at many DFT levels and no magic factor has to be used to fit experimental data. Such a situation is illustrated by some recent works[48,49] dealing with a comparison between DFT and sophisticated ab initio calculations like CCSD(T). They report that in average correlation functionals, like B3LYP or SVWN functionals, usually lead to reliable equilibrium geometries, vibrational frequencies, and energies for molecules like *n*-alkanes and X_2O and XYO with X, Y = Cl, Br. Many other theoretical works have been performed to determine the best functional form, like those performed recently by Handy's group and Chong's group.[50] As a general tendency, ab initio calculations present a larger sensitivity to the size of the basis set than DFT techniques. Thus, the results are expected to be highly improved by using an extended basis set, contrary to the DFT results. In the case of saddle points, the situation is not so clear due to the lack of systematic studies. Then, it is difficult to conclude about the ability of a DFT approach to get a full PES with the same degree of reliability for any geometrical configuration. At any event, tests on the quality of DFT functionals necessarily involve comparison with very good ab initio calculations taken as references.

VI. Wave Functions Analysis Associated with Some Saddle Points

An analysis of the changes of the wave functions on the reaction paths between the electronic structures of the asymptotic products and the intermediates which directly precede them can reveal the existence of conical intersections associated with saddle points when these intersections are avoided. The electronic analysis concerns the barriers labeled **2**, **2′**, **5**, **8**, **9**, **12**, **13**, **20**, **22**, **23**, and **23′** found along the asymptotic channels. Using simple valence bond type schemes sometimes coupled with molecular orbital (MO) calculations, we present in Figure 5a−g a qualitative interpretation of the electronic origin of these barriers. A similar analysis can be undertaken for the other saddle points which connect the intermediates, but the interpretation of their origin is much more difficult and even impossible with such crude models. In these figures, we have represented the atomic valence shell by three lines which mimic the p orbitals, the dots near them being their electronic occupancy. The s orbital is not explicitly drawn but only suggested by one or two dots representing its electronic occupancy. π orbitals are pictured by a line connecting two p orbitals. The number of unpaired electrons (they are explicitly shown by an arrow when necessary) has been selected to represent its state multiplicity according to the electronic distribution of the largest configuration state function (CSF) after CI calculation. The direction of approach between the two fragments obeys the linear or bent geometry of the intermediate formed. When this geometry is bent, we consider for simplicity a right angle of approach in the scheme in question.

Both barriers **2** and **2′** come from an avoided crossing between two sheets of potential associated with the asymptotic channels HCN($X^1\Sigma^+$) + O(^{3}P) and HCN($A^1\Pi$) + O(^{3}P). Figure 5a explains this situation. The collinear approach of the oxygen atom in its electronic ground state ^{3}P toward the N end of NCH($X^1\Sigma^+$) is not favorable because the interactions between a single electron of the oxygen atom and the electronic pairs of the nitrogen atom are repulsive (there is no unpaired electron in HCN). On the other hand, the interaction involving the first electronic excited state of HCN($A^1\Pi$) and O(^{3}P) is attractive; a single electron on the oxygen atom and a single electron on the nitrogen atom of opposite spin projection make the N−O σ bond feasible. It remains two unpaired electrons which keep the triplet multiplicity of the system. Hence, in a linear approach a true crossing occurs between two curves, but in a bent approach the cis and trans barriers **2** or **2′** arise from avoided crossings between these PES of the same symmetry and same multiplicity.

In Figure 5b, we interpret the origin of barrier **5** between the product channels HCO + N and the minimum **I**. Let us consider the approach of the N atom toward the O atom of HCO (bent) to form a trans configuration. The interaction between the electronic ground state of HCO(X^2A') and N(^{4}S) is repulsive due to the approach of an unpaired electron on the N atom toward an electronic pair on the O atom. But, the approach of N(^{2}D), which presents a vacant orbital toward the electron pair of the O atom, is favorable for the creation of a dative N−O bond. The triplet multiplicity is obtained by the presence of two unpaired electrons on the system. Once again an avoided crossing appears by interaction between repulsive and attractive potential energy sheets.

Interpretation of the origin of barriers **8** and **20** is a little bit more tricky. Both barriers come out from the approach at a right angle of the H(^{2}S) atom toward the N or C atom of NCO, respectively. Figure 5c.1 gives the electronic distribution of NCO($X^2\Pi$) with eight electrons in the σ orbitals and seven in the π ones. Analysis of the MO distribution shows that the unpaired electron is guided by a π orbital largely concentrated on the N atom, the coefficients of the 2p atomic orbitals in this MO being 0.84 on N, 0.30 on C, and −0.45 on O. Since NCO($X^2\Pi$) does not carry any other unpaired electron, the approach of H toward N or C to form a triplet state is repulsive. An

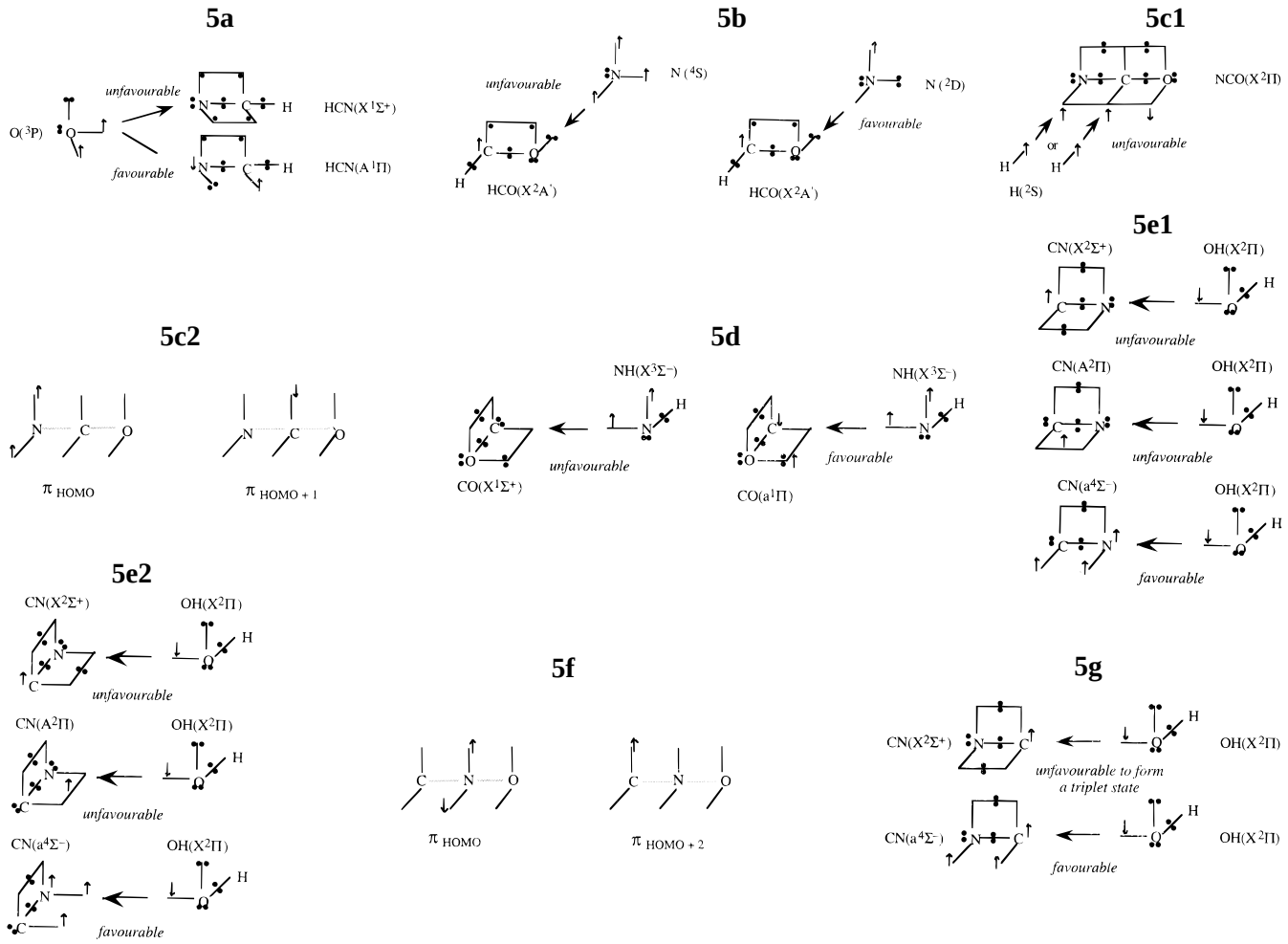

Figure 5.

attractive energy profile occurs from the interaction of low lying excited Π states of NCO with H(^{2}S). Such states are mainly described by the excitation of an electron from π orbitals localized on N atom (highest occupied molecular orbital, HOMO) and on O atom (HOMO − 1) to the π orbitals (HOMO + 1) localized on C atom, two other electrons being decoupled to keep a triplet multiplicity of the system. Figure 5c.2 shows the electronic distribution in the relevant π orbitals which can be associated with such Π states.

Barrier **9** arises from an avoided crossing between a repulsive potential surface associated with a repulsive interaction between NH($X^3\Sigma^-$) and CO($X^1\Sigma^+$) and an attractive one involving the first electronic excited state ($a^1\Pi$) of CO and NH($X^3\Sigma^-$) as shown in Figure 5d. As a matter of fact, the interaction between an electron guided by a p orbital of the nitrogen atom and the electron pairs of CO leads to a repulsive surface. Conversely, the promotion of a σ electron to an antibonding π^* orbital corresponding to the formation of CO($a^1\Pi$) creates a favorable interaction between NH and CO. Obviously, hybridization between s and p orbitals is necessary to explain the bent structure involving angles different from 90°.

The barrier associated with saddle point **12** can be described by the approach of OH at 90° with respect to CN on the N side (Figure 5e.1). But, the formation of the trans intermediate (**E**) from the saddle point structure **12** requires a rearrangement which can be roughly explained by a head to tail interaction between CN and OH (Figure 5e.2). The electronic structure of the trans intermediate (**E**) is a mixture of both approaches involving hybridization of s and p orbitals. The interaction between CN($X^2\Sigma^+$) and OH($X^2\Pi$) according to both orientations shown in Figure 5e.1,e.2 is basically repulsive. Attractive interaction between low lying excited states of CN and OH($X^2\Pi$) can be found with the participation of the CN($a^4\Sigma^-$) state. As a matter of fact, the CN($A^2\Pi$) state (which is lower in energy than the $a^4\Sigma^-$ state) implies, like the CN($X^2\Sigma^+$) state, a repulsive interaction (Figure 5e.1,e.2), since the unpaired electron of the p orbital of OH interacts either with an electron pair of CN or with an electron of same spin projection in order to conserve a global triplet multiplicity. The CN($a^4\Sigma^-$) state, characterized by three unpaired electrons, creates a favorable situation of coupling with the unpaired electron of OH in keeping the global triplet multiplicity.

The origin of barriers **13**, **23**, and **23′** can be found from the analysis of the CNO structure since **F**, **A**, and **B** intermediates require the formation of a bond between the H atom and the N and C atoms of CNO, respectively. The MO description of the ground state $X^2\Pi$ of CNO shows a structure having eight σ electrons and seven π ones similarly to NCO($X^2\Pi$). The unpaired electron is associated with a π orbital mainly localized on the N atom, the coefficients of the 2p orbitals being 0.5 on C, 0.7 on N, and −0.5 on O. The approach of a H atom toward the N or C atom of CNO is repulsive according to a global triplet multiplicity. On the contrary, the participation of Π excited states of CNO, which correspond to the promotion of an electron from the π HOMO to the π antibonding MO, creates a structure with three unpaired electrons interacting attractively with the H atom. Figure 5f shows the electronic distribution in the relevant π orbitals involved in these excited Π states.

Finally, the origin of barrier **22** can be found in a way similar to the interpretation of the appearance of barrier **12**. Figure 5g pictures the repulsive and attractive interactions which can be invoked when approaching OH toward the C atom of CN in

both $X^2\Sigma^+$ and $a^4\Sigma^-$ states to form the triplet structure of intermediate **H** via barrier **22**.

VII. Conclusions

The potential energy surfaces of singlet multiplicity for various isomers of the four-atomic H, C, N, and O system having already been extensively studied theoretically,[17−21] we have focused our interest on the study of the triplet potential energy surfaces. Our study, performed at several levels of calculation (semiempirical and ab initio), reveals the existence of a tiny barrier at the entrance channel on the singlet surface, a fact which was not reported previously in the literature. Consequently, the triplet surface would seem to play a major role in this reaction. Independently of the existence (or not) of this barrier, the triplet surface is 3-fold degenerate and must participate by at least 75% in the reaction with respect to the singlet surface.

From the analysis of the reaction paths obtained with these different approaches (at semiempirical level and at ab initio level), we find that the path leading to the exothermic formation of the products HCN + O is that possessing the smallest number of molecular rearrangements involving intermediate wells with very small barriers. The pathways leading to the very exothermic product channels NCO + H and CO + NH are also thermodynamically favorable in the reaction, but many more rearrangements are involved. These general results are consistent with the experimental findings, namely (i) the formation of HCN as major product of this reaction and (ii) the formation of NCO, CO, NH, and HCO to a much smaller extent. However, experimental and theoretical uncertainties remain concerning the formation of the products CN and OH.

Acknowledgment. This work has been largely carried out with the financial support of the European network:[22] Human Capital Mobility "Multichannel Reactions and Kinetic Modelling of Combustion Processes".

References and Notes

(1) Lanier, W. S.; Mulholland, J. A.; Beard, J. T. *21st Symposuim (International) on Combustion*; The Combustion Institute, 1988; p 1171.
(2) Chen, S. L.; McCarthy, J. M.; Heap, M. P.; Seeker, W. R.; Pershing, D. W. *21st Symposuim (International) on Combustion*; The Combustion Institute, 1988; p 1159.
(3) Miller, J. A.; Bowman, C. T. *Prog. Energy Combust. Sci.* **1989**, *15*, 287.
(4) Butler, J. E.; Fleming, J. W.; Goss, L. P.; Lin, M. C. *Chem. Phys.* **1981**, *56*, 355.
(5) Wagal, S. S.; Carrington, T.; Filseth, S. V.; Sadowski, C. M. *Chem. Phys.* **1982**, *69*, 61.
(6) Berman, M. R.; Fleming, J. W.; Harvey, A. B.; Lin, M. C. *19th Symposuim (International) on Combustion*; The Combustion Institute: Pittsburgh, PA, 1982; p 73.
(7) Lichtin, D.; Berman, M. R.; Lin, M. C. *Chem. Phys. Lett.* **1984**, *108*, 18.
(8) Dean, A. M.; Hanson, R. K.; Bowman, C. T. *J. Phys. Chem.* **1991**, *95*, 3180.
(9) Okada, S.; Yamasaki, K.; Matsui, H.; Saito, K.; Okada, K. *Bull. Chem. Soc. Jpn.* **1993**, *66*, 1004.
(10) Bocherel, P.; Herbert, L. B.; Rowe, B.; Sims, I.; Smith, I.; Travers, D. *J. Phys. Chem.* **1996**, *100*, 3063.
(11) Rieu, N-Q.; Henkel, C.; Jackson, J. M.; Mauersberger, R. *Astron. Astrophys.* **1991**, *241*, L33.
(12) Lindqvist, M.; Sandqvist, Aa.; Winnberg, A.; Johansson, L. E. B.; Nyman, L.-Å. *Astron. Astrophys. Suppl. Ser.* **1995**, *113*, 257.
(13) Lambrecht, R. K.; Hershberger, J. F. *J. Phys. Chem.* **1994**, *98*, 8406.
(14) Bozzelli, J. W.; Dean, A. M. *Combustion Chemistry*, 2nd ed.; 1994.
(15) (a) Kassel, L. S. *J. Phys. Chem.* **1928**, *32*, 1065. (b) Marcus, R. A.; Rice, O. K. *J. Phys. Colloid. Chem.* **1951**, *55*, 894.
(16) Takezaki, M.; Ohoyama, H.; Kasai, T.; Kuwata, K. *Laser Chem.* **1994**, *15*, 113.
(17) Poppinger, D.; Radom, L.; Pople, J. A. *J. Am. Chem. Soc.* **1977**, *99*, 7806.
(18) Yokoyama, K.; Takane, S.; Fueno, T. *Bull. Chem. Soc. Jpn.* **1991**, *64*, 2230.
(19) East, A. L. L.; Johnson, C. S.; Allen, W. D. *J. Chem. Phys.* **1993**, *98*, 2.
(20) Pinnavaia, N.; Branley, M. J.; Su, M.; Green, W. H.; Handy, N. C. *Mol. Phys.* **1993**, *78* (2), 319.
(21) Mebel, A. M.; Luna, A. M.; Lin, C.; Morokuma, K. *J. Chem. Phys.* **1996**, *105*, 15, 6439.
(22) (a) Groother, H. H., Ed. Multichannel Reactions and Kinetic Modelling of Combustion Processes. Proceeding and the Human Capital Mobility Meeting, October 1995 and September 1996. (b) Rowe, B., Ed. Structure and Reactivity of Molecular Ions. Proceedings of the Human Capital Mobility Meeting, May 1996.
(23) (a) Bergeat, A.; Loison, J. C.; Daugey, N.; Dorthe G. *Chem. Phys.*, in press. (b) Marchand, N.; Rayez, J. C.; Stoecklin, T. Manuscript in preparation.
(24) (a) Varandas, A. J. C. *Mol. Phys.* **1984**, *53*, 1303. (b) Varandas, A. J. C. *J. Mol. Struct. (THEOCHEM)* **1985**, *120*, 401. (c) Varandas, A. J. C. *Adv. Chem. Phys.* **1988**, *74*, 255.
(25) Dewar, M. J. S.; Thiel, W. *J. Am. Chem. Soc.* **1977**, *99*, 4899.
(26) (a) AMPAC 6.0, Semichem: Shawnee, KS. (b) Liotard, D. A. *Int. J. Quantum. Chem.* **1992**, *44*, 723.
(27) Rossi, I.; Truhlar, D. G. *Chem. Phys. Lett.* **1995**, *233*, 231.
(28) (a) Epstein, P. S. *Phys. Rev.* **1926**, *28*, 695. (b) Nesbet, R. K. *Proc. R. Soc.* (London) **1955**, *A230*, 312.
(29) Møller, C.; Plesset, M. S. *Phys. Rev.* **1934**, 618.
(30) (a) Broyden, C. G. *J. Inst. Math. Appl.* **1970**, *6*, 222. (b) Shanno, D. F. *J. Opt. Theory Appl.* **1985**, *46*, 87. (c) Shanno, D. F. *Math. Comput.* **1970**, *24*, 647. (d) Fletcher, R. *Comput. J.* **1970**, *13*, 317. (e) Goldfarb, D. *Math. Comput.* **1970**, *24*, 23.
(31) (a) Simons, J.; Banerjee, A.; Adams, N.; Shepard, R. *J. Phys. Chem.* **1985**, *89*, 52. (b) Baker, J. *J. Comput. Chem.* **1986**, *7*, 385. (c) Culot, P.; Dive, G.; Nguyen, V. H. *Theor. Chim. Acta* **1992**, *82*, 189.
(32) Liotard, D. A.; Perrot, J. P. In *Numerical Methods in the study of Critical Phenomena*; Spinger-Verlag: Berlin, 1981; p 213.
(33) Bockisch, F.; Liotard, D.; Rayez, J. C.; Duguay, B. *Int. J. Quantum. Chem.* **1992**, *44*, 619.
(34) However, nonzero minima of the cost function, corresponding to inflection points, can also be encountered on the PES.
(35) Fukui, K. *J. Phys. Chem.* **1970**, *74*, 4161.
(36) Miller, W. H.; Handy, N. C.; Adams, J. E. *J. Chem. Phys.* **1980**, *72*, 2.
(37) (a) Andersson, K.; Malmqvist, P. A.; Roos, B. O.; Sadlej, A. J.; Wolinski, K. *J. Phys. Chem.* **1990**, *94*, 5483. (b) Andersson, K.; Malmqvist, P. A.; Roos, B. O. *J. Chem. Phys.* **1992**, *96*, 1218.
(38) Dunning, T. H.; Hay, J. P. J. In *Modern Theoretical Chemistry*; Schaefer, H. F., III, Ed.; Plenum: New York, 1976; pp 1−28.
(39) Wahl, A. C.; Das, G. In *Modern Theoretical Chemistry*; Schaefer, H. F., III, Ed.; Plenum, New York, 1977; Vol. 3 (Methods of Electronic Structure Theory).
(40) (a) Brown, F. B.; Truhlar, D. G. *Chem. Phys. Lett.* **1985**, *117*, 307. (b) Varandas, A. J. C. *J. Chem. Phys.* **1989**, *90*, 4379.
(41) Andersson, K.; Roos, B. O. *Int. J. Quantum Chem.* **1993**, *96*, 591.
(42) Andersson, K.; Blomberg, M. R. A.; Fülscher, M. P.; Karlström, G.; Kellö, V.; Lindh, R.; Malmqvist, P.-Å.; Noga, J.; Olsen, J.; Roos, B. O.; Sadlej, A. J.; Siegbahn, P. E. M.; Urban, M.; Widmark, P.-O. MOLCAS-3; University of Lund: Lund, Sweden, 1994.
(43) (a) Miller, W. H. *J. Chem. Phys.* **1976**, *65*, 6. (b) Mozurkewich, M.; Benson, S. W. *J. Phys. Chem.* **1984**, *88*, 6429.
(44) Pau, C.-F.; Hehre, W. J. *J. Phys. Chem.* **1982**, *86*, 321
(45) Chre, M. W.; Davies, C. A.; Downey, J. R.; Frurip, D. J.; McDonald, R. A.; Syverud, A. N. JANAF Thermochemical Table, 3rd edition, *J. Phys. Chem. Ref. Data* **1985**, *14*.
(46) Bruna, P. *J. Chem. Phys.* **1980**, *49*, 39.
(47) Bowman, J. M.; Bittman, J. S.; Handing, L. B. *J. Chem. Phys.* **1982**, *85* (2), 911.
(48) (a) Ingamells, V. E.; Handy, N. C. *Chem. Phys. Lett.* **1996**, *248*, 373. (b) Chong, D. P.; Hu, C.-H.; Duffy, P. *Chem. Phys. Lett.* **1996**, *249*, 491. (c) Pulfer, M.; Hu, C.-H.; Chong, D. P. *Chem. Phys.* **1997**, *216*, 91. (d) Hu, C.-H.; Chong, D. P. *Chem. Phys.* **1997**, *216*, 99.
(49) Chaquin, P.; Bahou, M.; Schriver, A.; Schriver, L. *Chem. Phys. Lett.* **1996**, *256*, 609.
(50) Tsuzuki, S.; Uchimaru, T.; Tanabe, K *Chem. Phys. Lett.* **1995**, *246*, 9.